Urban Change Pattern Exploration of Megacities Using Multitemporal Nighttime Light and Sentinel-1 SAR Data

Meiqin Che, *Member, IEEE*, Anna Vizziello, *Senior Member, IEEE*, and Paolo Gamba, *Fellow, IEEE*

***Abstract*—During the last 20 years, fast urbanization activities have been highly concentrated in just few countries (e.g., China, India, and Nigeria) and have led to the emergence of large urban aggregations, with high population density. Still, very few researches have focused on this dynamic phenomenon with a global perspective using multisource remote sensing data. In this article, combining radar and spectral sensors of different spatial resolution, a novel approach based on a novel hierarchical biclustering technique is proposed and proved to be effective in discriminating the underlying change patterns without pre-estimating the number of clusters. To this aim, experimental results focused on newly emerging megalopolis in China, India, and Nigeria, as well as on the highly urbanized and stable Lombardy region in Italy, are presented. The analysis of the results allows us to understand, in a global and comparative perspective, the spatiotemporal differentiation of urban density and how cities are changing and evolving in the building volume and, to some extent, their economic level.**

***Index Terms*—Change pattern analysis, hierarchical biclustering (HBC), megalopolis, nighttime lights, Sentinel-1, synthetic aperture radar (SAR).**

I. Introduction

In THE past few decades, the emergence of megalopolises or megacities has already attracted great attention in investigating issues related to urbanization activities and planetary-scale changes [1], [2]. The research has mainly focused on early emerged megalopolis like Greater Tokyo Area [3], [4], Northeast megalopolis in the USA [5], and the Blue Banana megalopolis in Europe [6]. However, according to the "World Urbanization Prospects 2018" report from the United Nations, projections show that another 2.5 billion people will migrate from rural to urban areas by 2050, and nearly close to 90% of this expected increment is highly concentrated in just a few countries (India, China, and Nigeria) rather than in the most urbanized regions [7]. With much higher population density and larger urban agglomeration than existing megalopolises, the newly emerging ones confront more challenges in address housing, transportation, energy systems, microclimate change, and other environmental issues [8], [9]. Accordingly, in this article, newly emerging megalopolises are emphasized to further explore multidimensional changes due to urbanized aggregation or the merging of multiple cities.

Indeed, in recent years, a few papers have been devoted to investigate spatiotemporal aggregation [10]–[12] and/or socioeconomic changes within megalopolises [13], [14]; however, they only focused on urban extent monitoring and urban land use transformation using multispectral and nighttime light data. Although fusion techniques have been already employed in urbanization monitoring using heterogeneous datasets of different resolutions and modalities [15]–[17], there is still no work related to the use of synthetic aperture radar (SAR) data in conjunction with other sensors. SAR data provide useful hints about physical changes to the bi- and three-dimensional structure of the cities. Nighttime lights are a proxy to the economic development, the population density, and quite a few more social parameters [18], [19]. By using both datasets, we expect to be able to jointly consider changes due to urban expansion and those due to increasing socioeconomic activities. Following the research line presented in [20], in this article, we aim at combining Sentinel-1 (S1) SAR and Visible Infrared Imaging Radiometer Suite (VIIRS) nighttime measurements, to track both the 2-D/3-D urban expansion and its socioeconomic changes at the geographical scale of the so-called megacities or megalopolises.

Following [21], a "megalopolis" is a cluster of multiple urban areas, where, usually, the government policy aims at knitting the area together and promoting development through transportation and communication links. Since these areas are very large, and temporal patterns are a *a priori* unknown, unsupervised techniques are needed to analyze remote sensing data at their scale. Very few approaches have focused on unsupervised mapping of multipattern changes to understand complex urbanization phenomena. In our previous work [20], the joint use of heterogeneous sensors allows an unsupervised discovery of spatiotemporal features and deeper relationships between urban constructions and nighttime light changes, which reveal the connections between built-up area changes and socioeconomic development. However, a manual determination of these features' number is not easy to obtain in wide geographical areas, because it can be very large. Therefore, in order to better detect these meaningful

Manuscript received June 30, 2021; revised August 23, 2021 and September 26, 2021; accepted October 5, 2021. Date of publication October 12, 2021; date of current version November 1, 2021. The work of Meiqin Che was supported in part by the Fujian Technology Plan Project under Grant 2018Y0065. *(Corresponding author: Paolo Gamba.)*

Meiqin Che is with the School of Transportation and Civil Engineering, Nantong University, Nantong 226019, China (e-mail: lastrye00@gmail.com).

Anna Vizziello and Paolo Gamba are with the University of Pavia, 27100 Pavia, Italy (e-mail: anna.vizziello@unipv.it; paolo.gamba@unipv.it).

Digital Object Identifier 10.1109/JSTARS.2021.3119419

TABLE I
REMOTELY SENSED MEASUREMENTS (ALSO CALLED FEATURES) CONSIDERED IN THIS WORK

Features	Feature description
VV σ_0	VV polarization backscattering coefficient σ_0 of the SAR image at the starting date of the considered time interval
VH σ_0	VH polarization backscattering coefficient σ_0 of the SAR image at the starting date of the considered time interval
NL τ	Nighttime light data at the starting date of the considered time interval
VV $\Delta\sigma_0$	Change of the backscattering coefficient σ_0 (VV polarization) in the considered time interval
VH $\Delta\sigma_0$	Change of the backscattering coefficient σ_0 (VH polarization) in the considered time interval
NL $\Delta\tau$	Change of nighttime light data in the considered time interval

change patterns, in this work, a hierarchical biclustering (HBC) strategy is proposed to deal with unsupervised clustering at the geographical scale of a megalopolis.

The rest of this article is organized as follows. Section II introduces the proposed methodology by describing the HBC algorithm applied to the feature space extracted from the heterogeneous multitemporal data sequence. Section III reports and discusses the spatiotemporal change patterns extracted for newly emerging megalopolises. The results prove the robustness of the proposed approach for megalopolises of different urbanization levels and locations. Finally, Section IV summarizes the main findings and proposes some ideas about future research steps.

II. CHANGE PATTERN DETECTION WITH HBC

The procedure used in this work relies on the processing chain described in [20]. First of all, Sentinel-1 SAR is used to extract urban extents. This step ensures that the focus of the analysis is on built-up areas at the finest spatial resolution for freely available datasets. To handle Big Data over each megalopolis, which includes a cluster of geographically adjacent metropolitan areas that may be somewhat separated or merged into a continuous urban region, the critical preprocessing steps and computations are performed in Google Earth Engine [22]. Then, data-driven unsupervised classification is used to explore change patterns according to a feature space composed of the base and the change images. In this way, both the initial state and the temporal changes are considered.

To extract urban change patterns for these areas, the same datasets considered in [20] are exploited, i.e., SAR and nighttime light data. Specifically, the initial and difference data by SAR and nighttime light sensors, listed in Table I, are used. They are combined and analyzed according to the procedure described in the following.

Since the same pixels may have different discriminative uncertainty under different unsupervised classification methods, an ensemble of unsupervised clustering technique is introduced. Differently from [20], three different algorithms are jointly considered: K-means, Gaussian mixed model (GMM) with expectation maximization algorithm [23], and variational Bayesian Gaussian mixture (VBGM) [24]. These three techniques are applied to the same feature space. The procedure in [20] is resumed, and a 2-D change vector analysis is applied to interpret the clustering results. Considering the resolution difference between the nighttime light sensor and Sentinel-1 SAR, an upscaling is applied to the SAR images to match VIIRS images at 500-m resolution. However, in this article, due to the wide geographical area of analysis, which furthermore contains several metropolitan regions that are spatially disconnected, this vector analysis is performed at the object level, after each agglomerate of urban pixels is extracted by connected component analysis.

TABLE II
CLUSTERING STABILITY COMPARISON OF GMM, VBGM, K-MEANS, AND HBC

	GMM		VBGM		K-means		HBC	
	L1C1	L1C2	L1C1	L1C2	L1C1	L1C2	L1C1	L1C2
Tr(C)	42.55	16.14	47.83	19.98	42.23	16.57	41.03	12.46

A. Hierarchical Clustering

The performance of unsupervised classifiers depends on the data geometrical distribution in the feature space, as well as on the clustering principle they exploit. Accordingly, clustering applied to (very) heterogeneous data from different sources poses challenging issues with respect to the recognition of reliable clusters. Specifically, it may happen that a few observations often receive ambiguous class or cluster labels when multiple classifiers are applied to the same feature space. This is especially true for outliers or noisy measurements.

To avoid these issues, in this article, a hierarchical two-component clustering approach is applied to more reliably extract change patterns in urban built-up areas, according to the following procedure, schematically represented in Fig. 1.

1) *Initial clustering:* Starting from the whole dataset or a cluster, labeled "root cluster" or "parent cluster" in the layer Li, two clusters are obtained by binary-component clustering using K-means, GMM, and VBGM.
2) *Class label alignment:* For each classifier's clustered class, class centers are calculated and utilized to align cluster label by comparing the class center distances of subclasses between different classifiers.
3) *Cluster aggregation:* The generated layer (L_{i+1}) retains only "reliable" observations in clusters $L_{i+1}C_j$, where $j = \{1, 2\}$, and excludes "ambiguous" ones. The term "reliable" (see Fig. 2) means that the category assignment is consistent, i.e., the observation is assigned to clusters with very close cluster centers.
4) These steps are performed iteratively on "reliable" clusters generated at each layer.

The procedure eventually ends after a few iterations (three, in this article), providing reliable and unreliable clusters of data points. Further analysis is, therefore, focused only on reliable clusters, reducing misinterpretations.

As a matter of fact, this procedure improves the statistical consistency of the extracted clusters, which is shown quantitatively in Table II. The trace of the covariance matrices for the

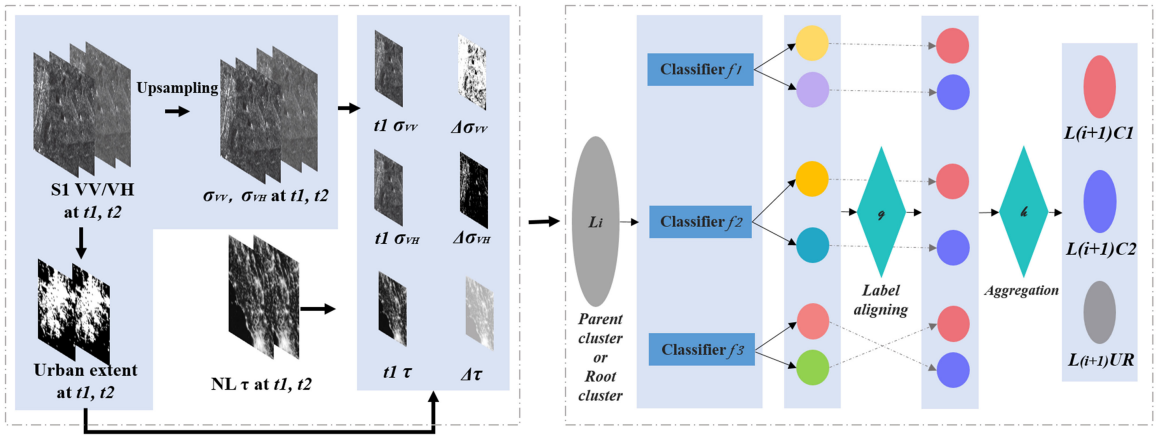

Fig. 1. Workflow of the urban change pattern exploration procedure used in this article.

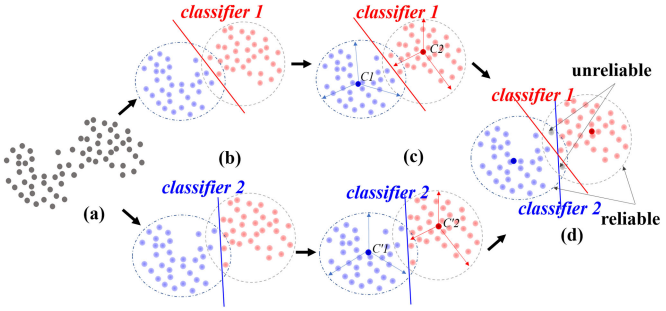

Fig. 2. Reliable clusters generated with multiple unsupervised classifiers. (a) Root or parent cluster. (b) Clustering by classifiers 1 and 2. (c) Cluster centers. (d) Reliable and unreliable clustered observations.

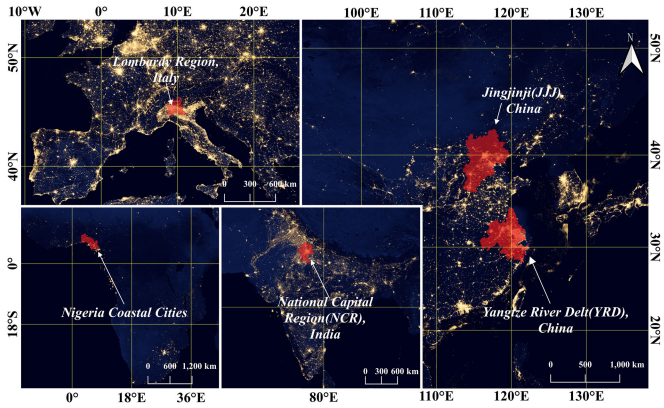

Fig. 3. Geographical location of the studied megalopolises.

label extracted at the first level (L_1) by K-means, GMM, and VBGM and the proposed approach are reported for one of our test cases. The values for the proposed HBC approach are the smallest ones.

III. Experimental Results

In this article, we focus on two megalopolises in China, namely, Jingjinji (JJJ) and Yangtze River Delta (YRD), one megalopolis in India, namely, the National Capital Region (NCR), and megacities in Nigeria, hence considering the currently most developed and the most densely populated portions in China, India, and Africa (see Fig. 3). These cities have boomed in population and economy for decades and are in the path to become the largest megalopolises in the world. Nigeria is the most populous country and the largest economy of 2018 in Africa. In this work, we focus on coastal cities, such as Lagos, Ibadan, and Port Harcourt, to understand the relationship between urban construction activities and economic activities.

In addition to these megalopolises in developing countries, we also select one comparative study area in a developed and fairly stable area: the mega metropolitan area of the Lombardy region in Italy. The rationale for this selection is that the Lombardy region is one of the most developed urban areas in Europe.

TABLE III
Megalopolises Studied and Data Acquisition Information

Megalopolis	Acquisition orbit	Acquisition time
YRD	Descending	Aug., Sept., Oct 2015 and 2018
J J J	Descending	Aug.,Sept., Oct 2015 and 2018
NCR	Descending	Jan., Feb., Mar. 2015 and 2018
Lombardy	Descending	Aug., Sept., Oct 2015 and 2018
Nigeria	Ascending	Aug., Sept., Oct 2015 and 2018

More specifically, the Milan metropolitan area in the Lombardy region, known as Greater Milan, is the largest metropolitan area in Italy. It includes the provinces of Milan, Bergamo, Como, Lecco, Lodi, Monza and Brianza, Pavia, Varese, and the Piedmontese Province of Novara, while some scholars also include the Province of Cremona and Brescia in Lombardy and the Emilian Province of Piacenza. The overall population under the narrowest definition is about 8.2 million over an area of about 13 000 km^2.

Table III lists the detailed information about the tested megalopolises in this article.

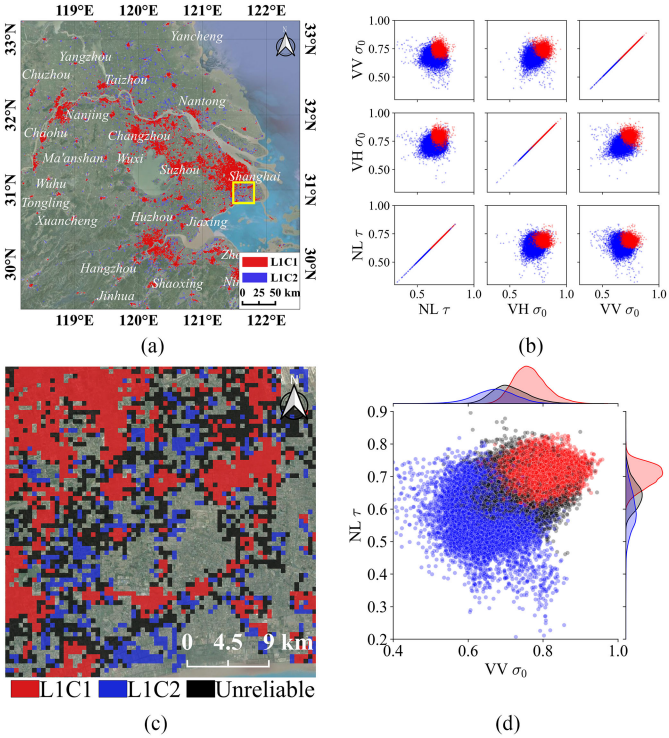

Fig. 4. YRD: (a) bidimensional scatterplot of the reliable clusters extracted in the first layer (L1) of the hierarchical clustering procedure; (b) spatial extents of the extracted clusters; (c) low confidence pixels (in black) for the subarea highlighted with a yellow rectangle in (a); and (d) corresponding scatterplot of all (clustered and low confidence) pixels, showing that low confidence pixels lay at the border between the reliable clusters.

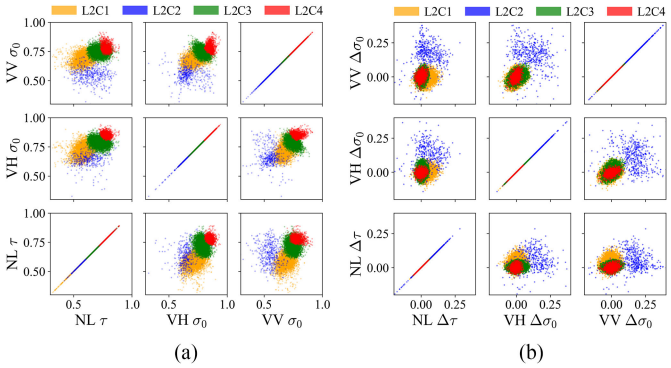

Fig. 5. YRD: bidimensional scatterplots of the clusters extracted in the second level of the hierarchical clustering procedure.

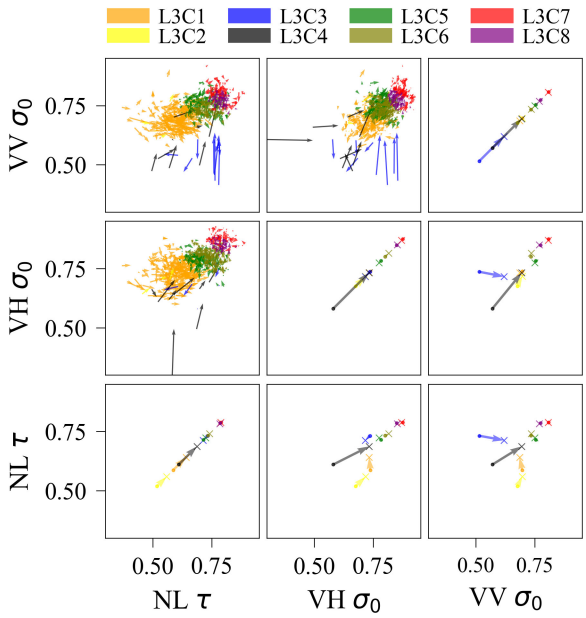

Fig. 6. Vector analysis for four-component clusters applied to YRD: the upper left corner is the set of vectors generated by randomly selecting samples; the lower right corner and the diagonal line utilize only use the cluster centers.

A. *Hierarchical Biclustering for YRD*

The first level of the hierarchical clustering procedure generates two clusters (L1C1 and L1C2), and the scatterplots for every possible feature pair of the YRD megalopolis are shown in Fig. 4(a), and the corresponding geographical area is visualized in Fig. 4(b). Specifically, Fig. 4(a) represents the projection of the retrieved two (red and blue) clusters in every possible 2-D subspaces of the base data. It is clear that the red and blue clusters correspond to different urban temporal patterns, and this is consistent with the spatial structure of these clusters for YRD in Fig. 4(a). The area in the red cluster has high building density at the starting date (base VV σ_0 and base VH σ_0) and a small change in any difference feature space (difference VV $\Delta\sigma_0$, difference VH $\Delta\sigma_0$, and difference NL $\Delta\tau$). Therefore, the red cluster may be interpreted as the core urban area, which did not change much in average during the considered time period. Instead, the blue cluster corresponds to low building density undergoing big changes and may be interpreted as the urban fringe subject to fast urban expansion.

In the second level (L2) of the hierarchical clustering, new clusters are obtained by separating the "parent clusters," and more detailed change patterns are revealed (see Fig. 5). The red and green clusters (L2C3 and L2C4) obtained from the red cluster (L1C1) in the upper level represent a further subdivision of the core area into its more stable part and the transition areas toward the fast developing urban fringe and are consistent with the well-known urban circle structure, e.g., in Beijing, and its pattern of urban outward expansion. Within a relative short time interval (in this work, we are considering the interval from 2015 to 2018), however, the expansion is limited. More obvious changes occur in villages and towns surrounding the main built-up area, which correspond to the yellow and blue clusters (L2C1 and L2C2) in Figs. 5 and 6, obtained from further clustering applied to the blue cluster (L1C2) in Fig. 4.

The four-component clusters allow recognizing more urban expansion patterns. Indeed, the blue and yellow clusters are discriminated, thanks to different change directions for the backscattering coefficient (i.e., the change in built-up structures). As shown in Fig. 7, the new constructions recognized as elements of the blue cluster (L2C2) commonly and frequently

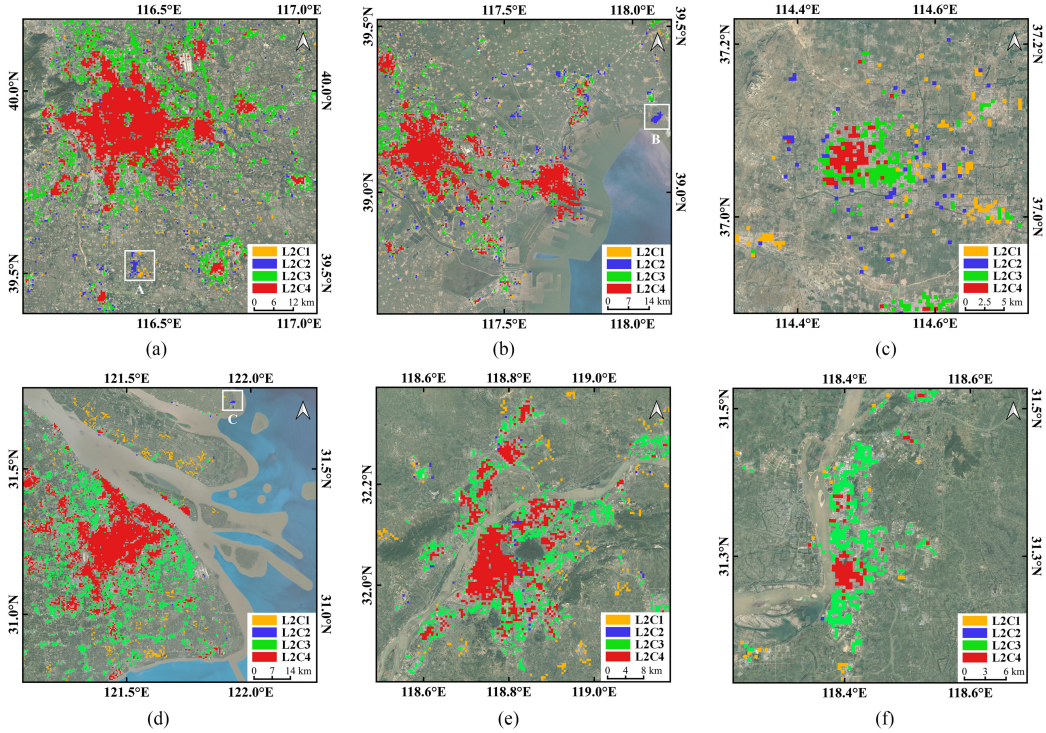

Fig. 7. Four-component clusters for multiple cities in JJJ and YRD megalopolises. (a) Beijing. (b) Tianjin. (c) Xingtai. (d) Shanghai. (e) Nanjing. (f) Wuhu.

occur beyond the suburban area and often accompany demolitions (recognized as elements of the yellow cluster).

Looking in more detail to the urban change patterns extracted by this technique, it is possible to appreciate that they are different depending on the urban size. For instance, among the two considered Chinese megalopolises, the expansion of cities with population over eight million people, such as Beijing, Tianjin, Shanghai, and Nanjing, is spatially discontinuous and starts from towns away from the main built-up area. Cities like Xingtai and Wuhu, which are smaller, spread randomly in all directions and more continuously in space.

B. Change Patterns for JJJ and YRD

Patterns are even more complex and rich of information when considering the third-level eight-component clustering. The aforementioned core urban areas (the red cluster in four components) are further separated into purple and red clusters (L3C7 and L3C8). Both clusters correspond to areas with almost no changes for these two megalopolises. They highlight instead highly developed infrastructures supporting a variety of entertainment and commercial activities. Finally, the suburban areas (subdivided into green and olive clusters) correspond to areas with lower building density and more low-rise buildings, with lighting facilities utilized to support the public transportation rather than entertainment and commercial activities.

As for the external and fast changing areas, the eight-component clustering helps to single out different changes in terms of feature magnitude and direction (increase or decrease). According to the physical properties of microwave polarization scattering, VH polarization signals mostly come from volume scattering of canopy and urban building blocks. Instead, VV polarization signals are mostly generated from double-bounce scattering among building blocks. These properties can be used to discriminate changes from urban areas with different building density. Accordingly, the blue cluster (L3C3) in Fig. 8(b) shows a 10–20% increase in VV σ_0 but does not exhibit any change in NL τ and VH σ_0, which means that there is no variation in the volume scattering, the spatial overflow, and the saturation of light. This effect can be explained with construction activities of low-density and low-rise building far from the main urban area. More detailed investigation can be found in Tables IV and V for YRD and JJJ megalopolises.

Comparing the spatial location of these changes (see Fig. 9), it becomes apparent that most construction activities has occurred far away from core urban areas: in airports, factories, ports, and villa districts.

C. Change Patterns of Coastal Cities in Nigeria and NCR in India

In Nigeria, the eight-clustering results show peculiar building and spatial configurations of these changes. As expected, they are different from those for Chinese megalopolises.

In this geographical area, the backscattering coefficient in core urban areas, represented by purple and red clusters, is below a relative value of 0.7, much smaller than the corresponding values for the cities in Chinese megalopolises. These low values are presumably due to the difference in building density. For instance, in China, more high-rise buildings are built than in

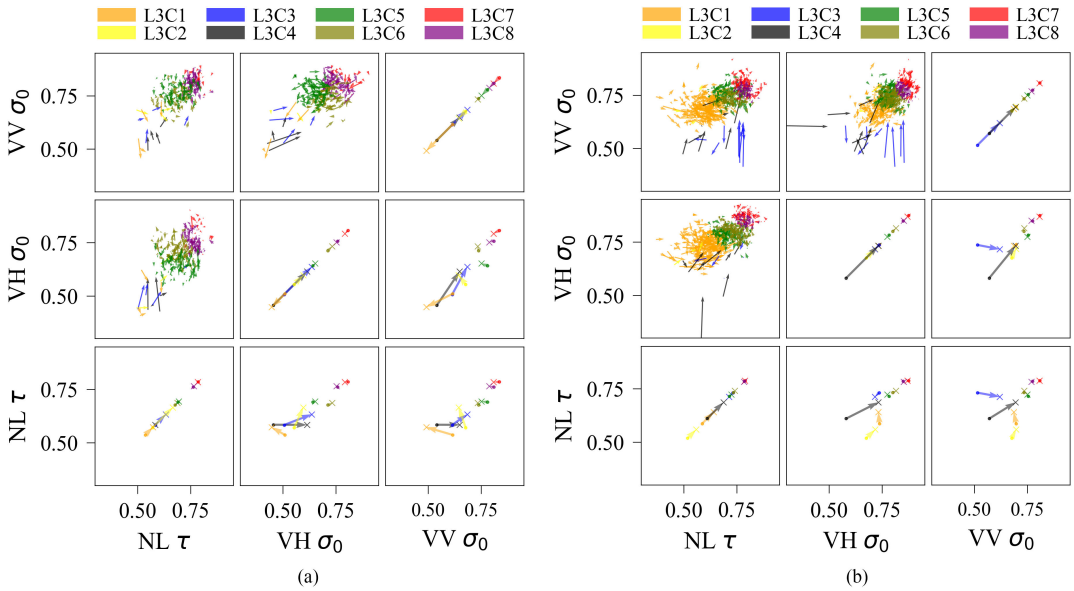

Fig. 8. Vector analysis for eight-component clusters of (a) JJJ and (b) YRD megalopolises: the upper left corner of (a) and (b) is the set of vectors generated by randomly selected samples; the lower right corner and the diagonal line of (a) and (b) utilize only the cluster centers.

TABLE IV
INTERPRETATION OF CHANGE PATTERNS IN YRD

Cluster	Initial state	Change description	Spatial description	Interpretation
Blue	High value in NL τ, low in backscattering power σ_0	10-20% increase in VV σ_0 Almost no change in NL τ and VH σ_0	Far away from urban area/river side/container terminal	Nearly complete construction of blocks with low building density. The economic and social activities have not yet followed up with urban expansion or construction.
Black	Median value in NL τ and backscattering powerσ_0	About 10-20% increase in VV σ_0 and VH σ_0 ,and 5-10% increase in NL τ	Seaside villas/ container terminal/ urban-rural fringe area	Construction of multi-storey and medium height houses with higher levels of building volumes and densities than the blue cluster.
Yellow	Medium or large value in NL τ, medium or large value in backscattering powerσ_0	About 1-5% increase NLτ, and almost no change in VV $\sigma_0$and VH σ_0	Rural areas	Relative high density of low-rise residential building blocks.
Orange	Medium value in NL τ and or medium value in backscattering powerσ_0	About 1-5% increase NL τ, and almost no change in VV σ_0 and VH σ_0	Rural areas	Relative low density of low-rise residential building blocks. Small town economic activities and factory production may bring increased light.

TABLE V
INTERPRETATION OF CHANGE PATTERNS IN JJJ

Cluster	Initial state	Change description	Spatial description	Interpretation
Blue	Medium value in NL τ, low in backscattering power σ_0.	About 10-15% increase in VV σ_0 and VH σ_0, and 1-5% decrease in NL τ.	urban-rural fringe area or away from urban areas.	Change from low-rise to high rise/residential extensions. The NL increase indicates a small increase in socio-economic activity.
Black	Medium or large value in NLτ, medium or large value in backscattering power σ_0.	About 10-20% increase in VV σ_0 and more in VH σ_0, and almost no increase in NL τ.	Sea side and away from urban areas	New constructions, such as factories and the new Beijing Daxing international airport.
Yellow	Medium value in NL τ and in backscattering powerσ_0.	No increase in VV σ_0 and subtle increase in VH σ_0, and 1-5% increase in NL τ.	Rural residents in countryside.	Lighting facility construction of airfield and small town economic development.
Orange	Medium or low value in NL τ, medium value in backscattering power σ_0.	About 5-10% decrease in VH σ_0 and more in VV σ_0, and almost no change in NL τ.	Away from urban areas.	Land leveling or demolition of old houses.

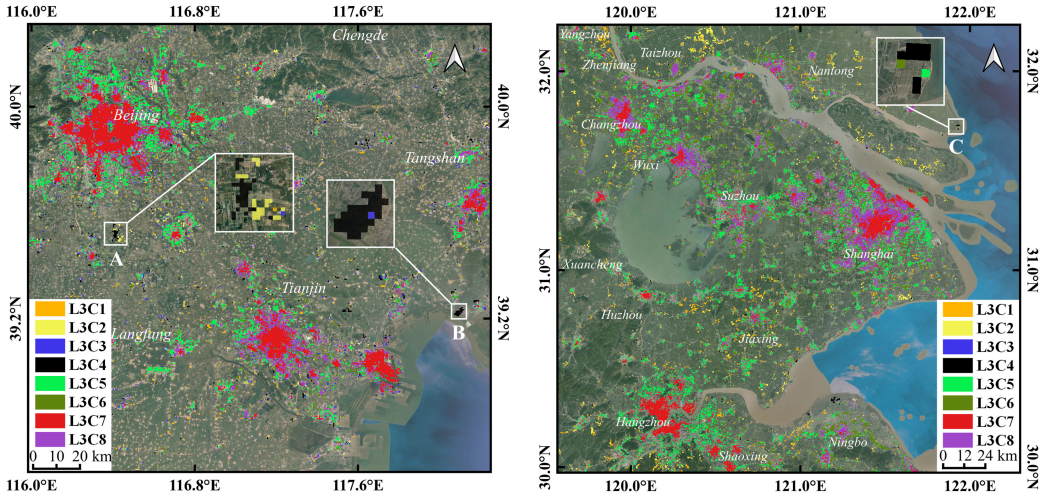

Fig. 9. Spatial mapping of clusters inside and outside urban areas. (a) Eight-component clustering map of JJJ. (b) Eight-component clustering map of YRD. Highlighted areas in the labeled patches correspond to change patterns shown in Fig. 10.

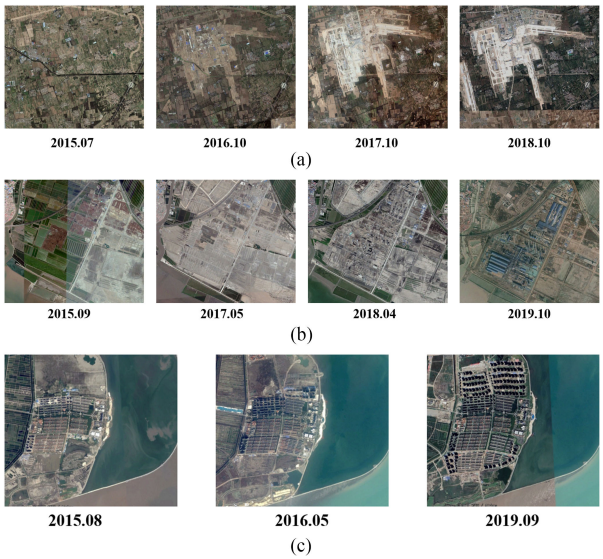

Fig. 10. Validating changes with Google Earth History Images. (a) Temporal change of Beijing Daxing International Airport labeled as patch A in Fig. 9(a). (b) Temporal change of the seaside factory labeled as patch B in Fig. 9(a). (c) Temporal change of seaside settlements labeled as patch C in Fig. 9(b).

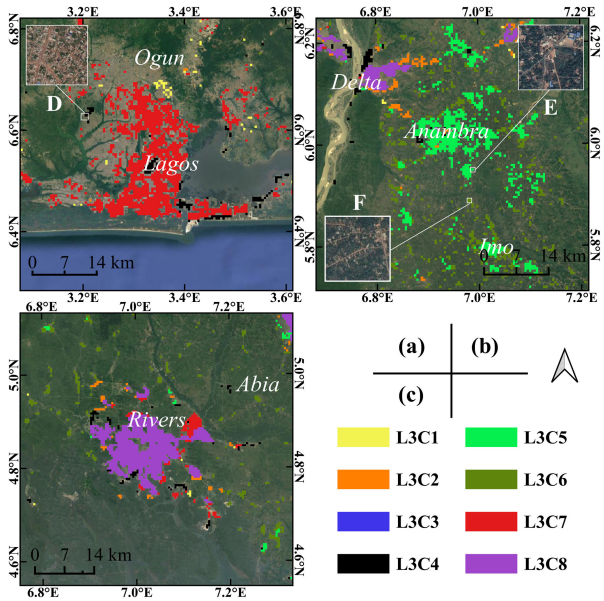

Fig. 11. Spatial representation of the eight-component third-level clusters for coastal cities in Nigeria. Highlighted areas in the labeled patches correspond to change patterns shown in Fig. 12.

other parts of the world, and this leads to larger backscattering coefficients.

The change vectors of the black cluster, increasing in VV and VH backscattering power in Fig. 13(a) and (b), indicate urban construction activities. However, the wide-range value of the scattering intensity and relatively high value of NL at the starting date suggest that the changes may have possibly happened inside urban core built-up areas and suburban built-up areas, as confirmed in Fig. 11, rather than outside the urban fringes in urban expansions, as typical in China. There are oil wells and refinery facilities, recognizable as black points far away from cities, with burning gas, singled out because of their very intense lights. The clustered pattern of blue and yellow vectors is recognized as rural areas and small towns (shown in Fig. 11) with great numerical fluctuation in NL. Although these large rural areas are spatially continuous and can be easily recognized as urban area, their illumination infrastructure is poor.

Figs. 13(d) and 14 illustrate the eight-component clustering result of NCR in India. Almost all clusters except the green one indicate decreasing trend in the backscattering coefficient, which might be caused by street facility degradation. The increase of blue cluster 7 and orange cluster 8 in terms of nighttime light

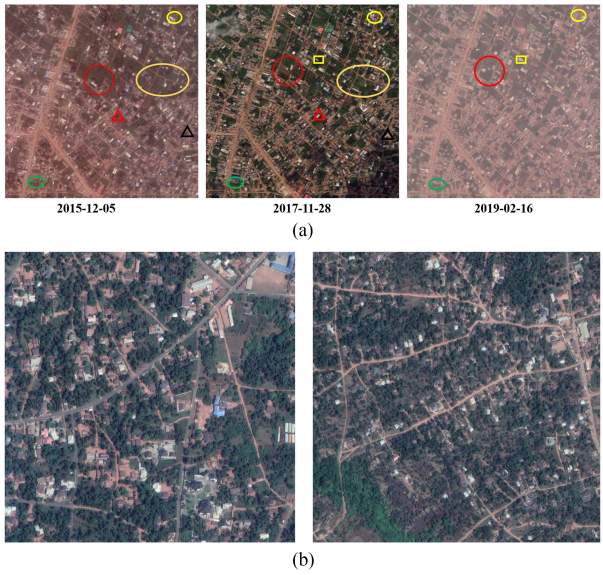

Fig. 12. Google Earth images of selected patches in Nigeria. (a) Density change of buildings labeled as patch D in Fig. 11(a) visualized by Google Earth Images. (b) Google Earth Images of patches E and F shown in Fig. 11(b).

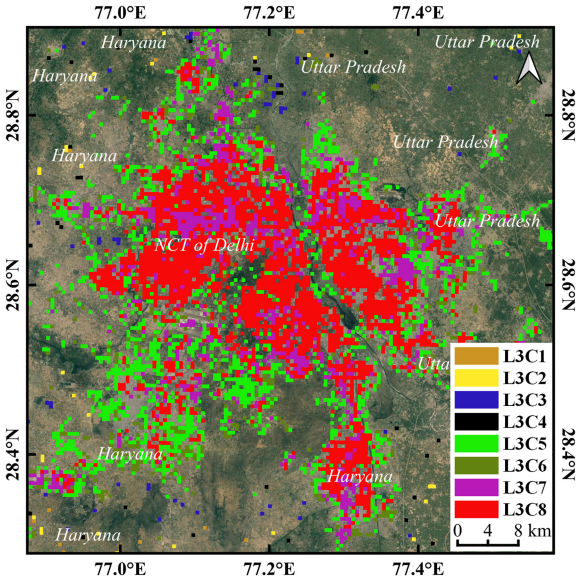

Fig. 14. Spatial representation of the eight-component third-level clusters for NCR in India.

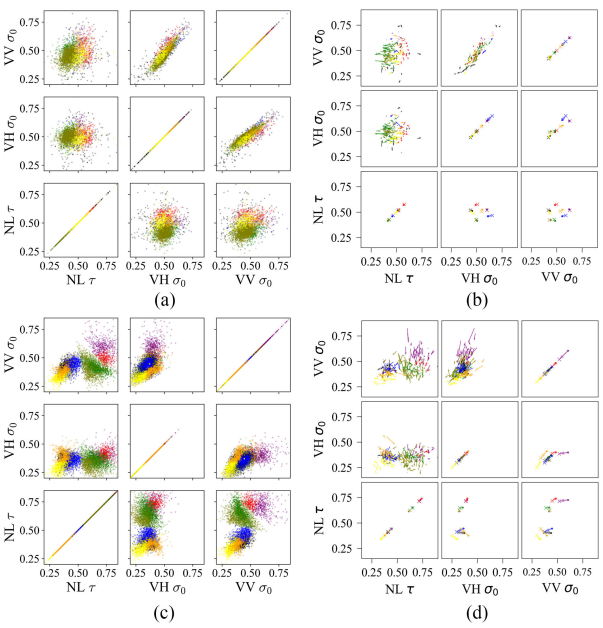

Fig. 13. Vector analysis of the eight-component clusters for coastal cities in Nigeria (first row) and NCR in India (second row). The upper left corner of (b) and (d) uses a subset of points; the lower right corner and the diagonal line of (b) and (d) only utilize only the cluster centers.

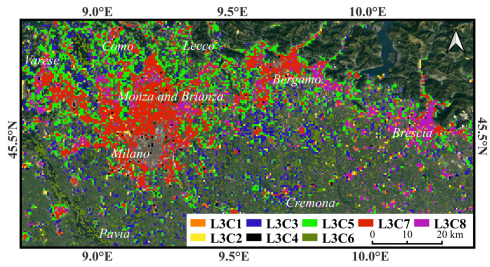

Fig. 15. Spatial representation of the eight-component third-level clusters for the Lombardy region in northern Italy.

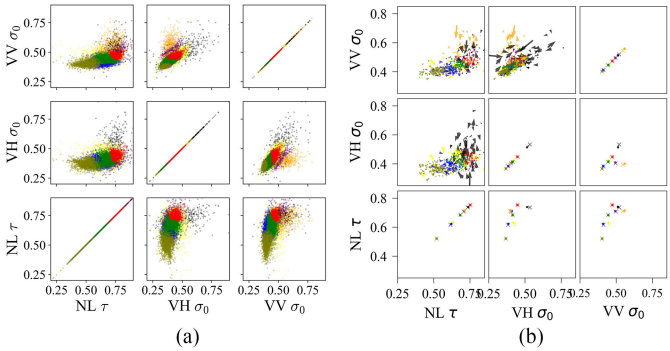

Fig. 16. (a) and (b) Vector analysis for the eight-component clusters for Milan metropolitan area: the upper left corner of (b) uses a subset of points; the lower right corner and the diagonal line utilize only the cluster centers.

implies a positive urbanization trend in terms of socioeconomic activities. However, these increases occur almost always far away from the Delhi urban area, showing that there is not much intraurban change activity.

D. Comparative Analysis and Validation of the Results

Applying the same procedure to the Lombardy urbanized area, it is possible to appreciate that built-up zones in the Milan metropolitan area are spatially compact and homogeneous (see Fig. 15). There is no clear distinction between Varese, Como, Milan, Bergamo, and Brescia. This suggests that the urbanization of Great Milan is mature, with a high urbanization level, above 70%. The very low growth rate results in few changes in both the SAR backscattering σ_0 and the nighttime light intensity

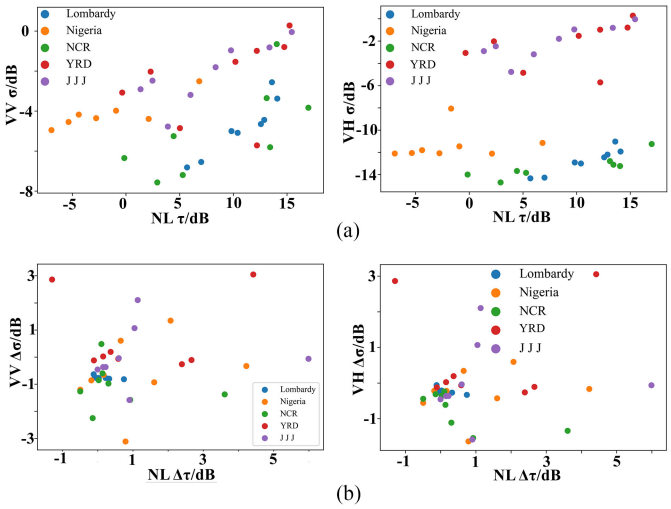

Fig. 17. (a) and (b) Initial state of the clusters for each megalopolis.

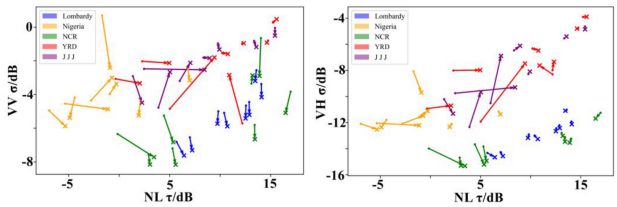

Fig. 18. Change vector analysis of the clusters for each megalopolis.

(see Fig. 16). Nevertheless, the black cluster still shows some minor changes caused by single building construction and maintenance (see Fig. 16). A higher backscattering coefficient or high reflectance indicates a higher urbanization level. As shown in Fig. 17(a), all megalopolises, excluding Nigeria, contain clusters with high socioeconomic level, measured by nighttime light reflectance. With respect to the backscattering coefficient, high values of VV polarization indicate higher building density in the form of high-rise building, which means more dense population in YRD and JJJ. The low-level clusters of the VH channel illustrate the low-rise building blocks of NCR and Lombardy, compared to the huge construction of high-rise building blocks in China.

The results in Figs. 17(b) and 18 illustrate the speed of urbanization from the perspective of nighttime lights and backscattering coefficients, as well as the consistency and inconsistency of real estate and economic activities during urbanization. The clusters of megalopolises in China show the largest change in nighttime light or backscattering coefficient, followed by the cities in India and Nigeria with a lower urbanization speed. One red-color cluster of YRD shows very fast real estate development but without any lighting facilities. In JJJ, certain urban areas only show a change in socioeconomic activities, presumably due to city block revitalization or new commercial building development. As the highly developed megalopolis, Lombardy almost indicates no change, as well as some other cities in both JJJ and YRD.

TABLE VI
VALIDATION OF THE URBAN EXTENTS AND RECOGNIZED CLUSTER

Megalopolis	Urban extents		Change detection	
	OA	K	Ł3 Change Clusters	Detected Rate
YRD	98.6%	0.93	L3C3/L3C4	86.7%
J J J	96.5%	0.86	L3C1/L3C3/L3C4	83.3%
NCR	86.9%	0.66	L3C3	66.7%
Nigeria	88.1%	0.76	L3C3	76.7%
Lombardy	95.5%	0.91	=	=

Aiming at validating the results of urban extents, we collected urban layers, including buildings and streets among the others, and nonurban layers, such as forest, farmlands, and other crop classes from Openstreetmap as ground truth, and the results are shown in Table VI.

The extracted urban extents directly impact the change due to the smaller percentage of changes that occur in urban areas. Changes like constructions or demolitions are validated by selecting an adequate number of objects, set equal to 30, within the cluster sets for each megalopolis. These areas have been visually verified as real changes.

IV. CONCLUSION

In this work, portions of urban areas with similar temporal patterns considering SAR and nighttime data are extracted by using a novel bihierarchical clustering approach. Then, an object-oriented vector analysis is implemented by exploiting the extracted clusters. This analysis allows us to interpret the temporal patterns generated by the proposed approach and characterize effectively different urban changes inside megacities.

The approach was tested on fast-developing urban areas in China, India, and Nigeria, as well as in areas of developed countries, such as the Lombardy region in Italy. The experimental results confirm the effectiveness of the proposed method in mapping multipattern changes using remote sensing data from heterogeneous sources.

More specifically, the main conclusions of this work are as follows.

1) The implemented HBC producer leads to more reliable clusters and highlights interesting urban change patterns referring to both construction/demolition of built-up structures and, to some extents, changes in the economic activity, represented as proxy by the nighttime lights.
2) Thanks to the joint use of the initial values and the temporal change, the detected patterns are clearly differentiated among core urban, suburban areas, and areas beyond urban outskirts. Specifically, settlement areas with very recent developments are singled out and clearly recognized.
3) There exists a high correlation between VV and VH polarization when downscaling Sentinel-1 SAR data to the nighttime light spatial resolution, suggesting that polarization is critical for analyses at the finest resolution, but not at the megacity scale.
4) Building density and infrastructure constructions are the main differences between highly urbanized areas (e.g., Milan), median-urbanized areas (e.g., Nanjing and inner

cities in China), and less-urbanized areas (e.g., Onitsha and coastal cities in Nigeria).

5) The time frame used for the analysis is crucial. A few years are not enough to capture changes in stable urban areas of developed countries, while they are useful to discriminate multiple different change patterns in very dynamic growing economies. Since the Sentinel constellation is meant to stay, more complex temporal change patterns will become decipherable in the near future.

REFERENCES

[1] K. C. Seto and D. Satterthwaite, "Interactions between urbanization and global environmental change," *Current Opinion Environ. Sustain.*, vol. 2, pp. 127–128, 2010.

[2] R. J. Nicholls, "Coastal megacities and climate change," *GeoJournal*, vol. 37, no. 3, pp. 369–379, 1995.

[3] R. Ohtsuka and M. Umezaki, "Changing population structure and commuting situation in Tokyo megalopolis: A municipality-based analysis," *J. Human Ergol.*, vol. 22, no. 1, pp. 69–73, 1993.

[4] N. Y.-p. Chen and L. Heligman, "Growth of the world's megalopolises," in *Mega-City Growth and the Future*. Tokyo, Japan: United Nations Univ. Press, 1994, pp. 242–261.

[5] J. Gottmann, *Megalopolis: The Urbanized Northeastern Seaboard of the United States*. New York, NY, USA: Twentieth Century Fund, 1961.

[6] T. Mori, "A modeling of megalopolis formation: The maturing of city systems," *J. Urban Econ.*, vol. 42, no. 1, pp. 133–157, 1997.

[7] *2018 Revision of World Urbanization Prospects*, United Nations Department of Economic and Social Affairs, New York, NY, USA, 2018. [Online]. Available: https://www.un.org/development/desa/publications/2018-revision-of-world-urbanization-prospects.html

[8] Y. Lin, A. Liu, E. Ma, X. Li, and Q. Shi, "Impacts of future urban expansion on regional climate in the Northeast megalopolis, USA," *Adv. Meteorol.*, vol. 2013, 2013, Art. no. 362925.

[9] H. J. Van Ginkel and P. J. Marcotullio, "Asian urbanization and local and global environmental challenges," in *Managing Urban Futures*. Milton Park, U.K.: Routledge, 2016, pp. 27–52.

[10] H. Taubenböck, M. Wiesner, A. Felbier, M. Marconcini, T. Esch, and S. Dech, "New dimensions of urban landscapes: The spatio-temporal evolution from a polynuclei area to a mega-region based on remote sensing data," *Appl. Geogr.*, vol. 47, pp. 137–153, 2014.

[11] T. Ramachandra, B. H. Aithal, and S. Sreekantha, "Spatial metrics based landscape structure and dynamics assessment for an emerging Indian megalopolis," *Int. J. Adv. Res. Artif. Intell.*, vol. 1, no. 1, 2012.

[12] H. Taubenböck *et al.*, "Urban structure analysis of mega city Mexico city using multisensoral remote sensing data," in *Proc. SPIE*, vol. 7110, 2008, Art. no. 71100E.

[13] Y. Chen, X. Li, Y. Zheng, Y. Guan, and X. Liu, "Estimating the relationship between urban forms and energy consumption: A case study in the pearl river delta, 2005–2008," *Landscape Urban Planning*, vol. 102, no. 1, pp. 33–42, 2011.

[14] C. Yang *et al.*, "A spatial-socioeconomic urban development status curve from NPP-VIIRS nighttime light data," *Remote Sens.*, vol. 11, no. 20, 2019, Art. no. 2398.

[15] H. Taubenböck, T. Esch, A. Felbier, M. Wiesner, A. Roth, and S. Dech, "Monitoring urbanization in mega cities from space," *Remote Sens. Environ.*, vol. 117, pp. 162–176, 2012.

[16] A. Salentinig and P. Gamba, "Multiscale multisensor decision level data fusion for urban mapping," in *Proc. 4th Int. Workshop Earth Observ. Remote Sens. Appl.*, 2016, pp. 67–71.

[17] R. Padmanaban, A. K. Bhowmik, and P. Cabral, "Satellite image fusion to detect changing surface permeability and emerging urban heat islands in a fast-growing city," *PLoS One*, vol. 14, no. 1, 2019, Art. no. e0208949.

[18] S. Frolking, T. Milliman, K. C. Seto, and M. A. Friedl, "A global fingerprint of macro-scale changes in urban structure from 1999 to 2009," *Environ. Res. Lett.*, vol. 8, no. 2, 2013, Art. no. 024004.

[19] X. Huang, A. Schneider, and M. A. Friedl, "Mapping sub-pixel urban expansion in China using MODIS and DMSP/OLS nighttime lights," *Remote Sens. Environ.*, vol. 175, pp. 92–108, 2016.

[20] M. Che and P. Gamba, "Intra-urban change analysis using Sentinel-1 and nighttime light data," *IEEE J. Sel. Topics Appl. Earth Observ. Remote Sens.*, vol. 12, no. 4, pp. 1134–1142, Apr. 2019.

[21] B. Wang and J. Zheng, "Research on the evaluation of land intensive utilization in megalopolis of China," *J. Univ. Sci. Technol. Beijing (Soc. Sci. Ed.)*, vol. 22, pp. 24–28, 2006.

[22] J. Rutkowski, M. J. Canty, and A. A. Nielsen, "Site monitoring with Sentinel-1 dual polarization SAR imagery using Google Earth Engine," *J. Nucl. Mater. Manage.*, vol. 46, no. 3, pp. 48–59, 2018.

[23] F. Pernkopf and D. Bouchaffra, "Genetic-based EM algorithm for learning Gaussian mixture models," *IEEE Trans. Pattern Anal. Mach. Intell.*, vol. 27, no. 8, pp. 1344–1348, Aug. 2005.

[24] D. M. Blei, A. Kucukelbir, and J. D. McAuliffe, "Variational inference: A review for statisticians," *J. Amer. Stat. Assoc.*, vol. 112, no. 518, pp. 859–877, 2017.

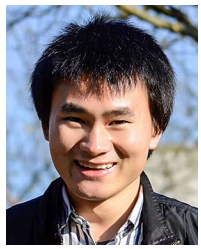

Meiqin Che (Member, IEEE) received the B.S. degree in resources environment and management of urban and rural planning from Northwest University, Xi'an, China, in 2008, the M.S. degree in cartography and geography information systems from Nanjing University, Nanjing, China, in 2016, and the Ph.D. degree in electronics, computer and electrical engineering from the University of Pavia, Pavia, Italy, in 2020.

He is currently a Lecturer with the School of Transportation and Civil Engineering, Nantong University, Nantong, China. His current research interests include polarimetric synthetic aperture radar (SAR) image processing, SAR time-series analysis, change detection, and urban remote sensing.

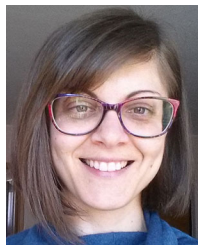

Anna Vizziello (Senior Member, IEEE) received the Laurea degree in electronic engineering and the Ph.D. degree in electronics and computer science from the University of Pavia, Pavia, Italy, in 2007 and 2011, respectively.

She is currently a Senior Research Associate with the Telecommunication and Remote Sensing Laboratory, University of Pavia. From 2007 to 2009, she also collaborated with the European Centre for Training and Research in Earthquake Engineering working with the Telecommunications and Remote Sensing group. She was a Visiting Researcher with the Broadband Wireless Networking Lab, Georgia Institute of Technology, Atlanta, GA, USA, from 2009 to 2010, with the Universitat Politécnica de Catalunya, Barcelona, Spain, in Summer 2009 and 2010, and with Northeastern University, Boston, MA, in Winter 2011 and in Summer 2016. She has been included in the 2018 list of "N2Women: Rising Stars in Computer Networking and Communications" for outstanding and impactful contributions in the area of networking/communications, supported by the IEEE Communication Society. Her research interests include wireless communication and sensor systems.

Paolo Gamba (Fellow, IEEE) received the Laurea (*cum laude*) and Ph.D. degrees in electronic engineering from the University of Pavia, Pavia, Italy, in 1989 and 1993, respectively.

He is currently a Professor with the University of Pavia, where he leads the Telecommunications and Remote Sensing Laboratory. He has been invited to give keynote lectures and tutorials in several occasions about urban remote sensing, data fusion, Earth observation data for physical exposure, and risk management. He authored or coauthored more than 170 papers in international peer-reviewed journals and presented 310 research works at workshops and conferences.

Dr. Gamba was the Editor-in-Chief for IEEE GEOSCIENCE AND REMOTE SENSING LETTERS from 2009 to 2013 and the Chair of the Data Fusion Committee of the IEEE Geoscience and Remote Sensing Society (GRSS) from October 2005 to May 2009. He has been elected in the GRSS Administrative Committee since 2014, was the GRSS President from 2019 to 2020, and is currently the GRSS Junior Past President. He has been the organizer and Technical Chair of the biennial GRSS/ISPRS Joint Workshops on "Remote Sensing and Data Fusion over Urban Areas" from 2001 to 2015. He was also the Technical Co-Chair of 2010, 2015, and 2020 IEEE International Geoscience and Remote Sensing Symposium, in Honolulu (HI, USA), Milan (Italy), and online, respectively.